



UNIVERSITY OF
BIRMINGHAM

Electrochemical Characterisation of thiols and di-sulphide Modified Gold Nanoparticles in a Physiological Medium

Roshni Mistry

Supervisor: **Dr P. Rodriguez**

Co Supervisor: **Dr F Fernandez-Trillo**

Masters Thesis

MSc by Research

School of Chemistry, University of Birmingham, Edgbaston, UK, 2018.

UNIVERSITY OF
BIRMINGHAM

University of Birmingham Research Archive

e-theses repository

This unpublished thesis/dissertation is copyright of the author and/or third parties. The intellectual property rights of the author or third parties in respect of this work are as defined by The Copyright Designs and Patents Act 1988 or as modified by any successor legislation.

Any use made of information contained in this thesis/dissertation must be in accordance with that legislation and must be properly acknowledged. Further distribution or reproduction in any format is prohibited without the permission of the copyright holder.

Dedication

I would like to dedicate this thesis to my mother, Jyotsna. She has supported me throughout this journey and has given me valuable advice throughout my education, always telling me to never give up and always carry on doing what I love.

Acknowledgements

I would like to personally thank my supervisor Dr Paramaconi Rodriguez and co-supervisor Dr F Fernandez-Trillo for all the guidance and support that they have given me over the past two years. Also, I thank them for the opportunity to be able to carry out this project.

I also thank Adam Kolodziej and Javier Monzo for all the help with my experimental studies during my Masters.

Abstract

Many different biosensors are currently used in medicinal applications to help detect pathogens and toxins.¹ Current techniques, such as PCR (polymerase chain reaction) and immunological based detection lack in versatility, are expensive and complicated to use.²⁻⁴ Due to these limitations, there is an increasing need for rapid, real-time, selective and low cost techniques.⁵

Advancements in nanotechnology and the use of surface modified gold nanoparticles could potentially overcome these present-day limitations, leading to new areas of detection using nano-biosensors.¹

In addition, the use of electrochemical biosensors have successfully been used in the detection of bacteria and pathogens without many of the limitations listed above. Electrochemical biosensors are based on the idea that electrochemical species, such as electrons, are consumed or generated and produce an electrochemical signal; which can be measured by an electrochemical detector.⁶

Here, gold nanoparticles were synthesized by the colloidal seed mediated method. The characterisation of gold nanoparticles were performed by UV-Vis, TEM, SEM and XRD. The electrochemical cleansing of the gold nanoparticles was also characterised by using Pb underpotential deposition.

In order to make a platform to detect toxins, modification was required to the gold nanoparticles in order to start designing the building blocks of the electrochemical biosensor.

The stability of the functionalised gold nanoparticles by molecules 1,4-dithiothreitol, thioctic acid and 3-mercaptopropionic acid were monitored by cyclic voltammetry, whilst in a neutral medium. From the three different molecules, experiments demonstrate that the disulphides are more stable at negative potentials in comparison to the thiol, as a result of having two coordinating sulphur atoms in their structure.

The most stable thiol or disulphide is most desirable as the fundamental part of the sensor is the sulphur containing molecule. From all three molecules, thioctic acid desorption from the electrode surface occurred at the lowest potentials, therefore the most stable and most suitable out of three molecules if used for sensing.

Contents

Abstract.....	6
List of abbreviations	10
Chapter 1:.....	11
Introduction to the use of nanoparticles as electrochemical biosensors	11
1.1: Introduction.....	11
1.2: Current bio-sensing technology	12
1.2.1: Culture and colony	12
1.2.2: Polymerase chain reaction (PCR)	12
1.2.3: Immunological based detection	13
1.3: Electrochemical sensing	13
1.3.1: Potentiometric sensors.....	14
1.3.2: Amperometric sensors	15
1.3.3: Conductometric sensors.....	15
1.4. Nanoparticles and their physical and chemical properties.....	16
1.4.1 Sensing of Bacterial pathogens.....	16
1.4.2: Gold nanoparticles as electrochemical biosensors	17
1.5: Previous synthesis methods of gold nanoparticles.....	18
1.5.1: Physical methods	18
1.5.1.1: Electron beam lithography	18
1.5.1.2: Photolithography.....	19
1.5.2: Chemical methods	20
1.5.2.1: The Turkevich method	20
1.5.2.2: The Brust Method	21
1.5.2.3: Seeded growth method.....	21
1.6 Conclusion.....	21
Chapter 2:.....	23

Synthesis, growth and characterisation of Gold Nanoparticles	23
2.1: Introduction.....	23
2.2: Experimental approach.....	23
2.2.1: Synthesis of Gold Nanoparticles	23
2.2.2: Chemical cleaning method of Gold Nanoparticles	24
2.3: Principles of characterisation of Gold Nanoparticles	25
2.3.1: Characterisation by UV-Vis	25
2.3.2: Characterisation by X-Ray Diffraction.....	27
2.3.3: Characterisation by Transmission Electron Microscopy.....	27
2.4 Conclusions.....	28
Chapter 3: Electrochemical Cleaning and Characterisation of Gold Nanoparticles.....	29
3.1: Fundamentals of Electrochemical Characterisation by Cyclic Voltammetry	29
3.1.1: What is Cyclic Voltammetry	29
3.1.2: Reversible and Irreversible systems	32
3.2: Electrochemical set-up	35
3.2.1: Cleaning of the Glassy Carbon electrode	36
3.2.2: Preparation of Gold Nanoparticle coated working electrode	37
3.3: Electrochemical Cleaning and Characterisation of Gold Nanoparticles using Pb Under Potential Deposition.....	38
3.3.1: Cleaning of gold nanoparticles by Lead UPD	38
3.4: Conclusions.....	42
Chapter 4: Electrochemical stability of modified gold electrodes	43
4.1: Introduction.....	43
4.1.1: The chemistry of 1,4-dithiothreitol.....	43
4.2: Experimental procedure:.....	44
4.2.1: Surface modification of gold electrode using 1,4-dithiothreitol, thiocetic acid and 3- mercaptopropionic acid.....	44
4.3: Electrochemical characterisation	45
Introduction	45

4.3.1: Electrochemical characterisation of 1,4-dithiothreitol.....	47
4.3.1.1: Conclusion	47
4.3.2: Electrochemical characterisation of Thiocetic acid	48
4.3.1.1: Conclusion	48
4.3.3: Electrochemical characterisation of 3- mercaptopropionic acid	48
4.3.1.1: Conclusion	49
Chapter 5: Conclusion and outlook:	50
References	51
Appendix:.....	55

List of abbreviations

The table below lists the abbreviations and acronyms used throughout the thesis. For abbreviations that are not in common use, the full term is also mentioned where it is first used in the text.

Abbreviation	Meaning
AuNPs	Gold nanoparticles
PCR	Polymerase chain reaction
EIA	Enzyme immunoassay
ELISA	Enzyme linked immunosorbent assay
ELFA	Enzyme linked fluorescent assay
EBL	Electron beam lithography
UV	Ultraviolet
HAuCl ₄	Chloroauric acid
NaBH ₄	Sodium Borohydrate
CTAB	Cetyltrimethylammonium bromide
SAM	Self-assembly monolayer
ISE	Ion-selective electrodes
MPA	3-mercaptopropionic acid
SCE	Saturated calomel electrode
RHE	Reversible hydrogen electrode

Chapter 1:

Introduction to the use of nanoparticles as electrochemical biosensors

1.1: Introduction

Factors such as food intoxication and contaminated water supplies are a few of the many reasons for infectious diseases being a serious healthcare problem in the world today.⁷ As a consequence, there is a substantial rate of morbidity and mortality due to such pathogens in water.⁸ In developing countries, infectious diseases cause up to 40% of the deaths.⁹

A common way of detecting bacteria and pathogens is by using biosensors. A biosensor is an analytical device, which in a living environment can detect chemical and biological compounds. These molecular techniques exist because their studies can deliver epidemiological information to trace for the source of human infections. There are numerous diverse biological recognition elements, which purposely change upon binding with a specific compound. That specific 'change' is then converted into a signal that can be analysed further. The different changes are then translated into a signal which is detected via optical, electrochemical, calorimetric, acoustic, piezoelectric magnetic and micromechanical transducers.^{4,10-12}

Current biosensors and their methods of detection of pathogens are very expensive and time consuming. The detection of target pathogens requires development of highly specific and sensitive methods to overcome their current draw backs.¹

In this thesis, gold nanoparticles were synthesized, characterised and then later modified by adding three different sulphur-containing molecules. The first chapters focus on monitoring the stability of the nanoparticles, as it is only when they reached a preferred size they were modified with the sulphur containing molecules. Chapter 4 depicts the next focus, analysing the electrochemical stability of the modified gold nanoparticles. These were the first steps taken in order to anticipate the wider goal of creating an electrochemical biosensor.

1.2: Current bio-sensing technology

Traditional methods for the detection and identification of pathogenic bacteria specifically depend on microbiological and biochemical identification. Many of these different characterising methods can be sensitive; the majority are expensive and give both qualitative and quantitative information depending on the numbers and nature of the microorganisms tested.

The most popular techniques for pathogen detection are colony counting method, polymerase chain reaction (PCR) and immunology methods. They each involve counting of bacteria, DNA analysis and antigen-antibody interactions respectively.^{4,7,12}

1.2.1: Culture and colony

Culture and colony based methods are currently the most reliable and accurate, as well as the oldest, amongst the different techniques for pathogen detection.^{4,13,14} However, this method is time consuming, where in some circumstances up to 72 hours are required to obtain results. The time to develop a colony varies, as for example a colony containing 10^6 organisms will take between 18 – 24 hours.^{13,14}

After the bacteria has been cultivated, there are a range of different selective media. These can be used to detect specific bacteria species that can contain inhibitors, or particular substrates which only the targeted bacteria can degrade, or that confers a particular colour to the growing colonies. The methods for detection are then carried out via optical methods such as ocular inspection.⁴

1.2.2: Polymerase chain reaction (PCR)

PCR is a common bacterial detection method, which uses nucleic acid amplification technology, developed in the mid 1980's.¹³ It has successfully been shown to accurately detect small amounts of microbial pathogens such as viruses, bacteria, protozoa and helminthes.³ The method is based on isolation, amplification and quantification of a short DNA sequence, including the targeted bacteria's genetic material.⁴ It is a developing and promising method as it detects the organism by amplifying the target rather than the signal,^{10,13,14} therefore it is less likely to produce a test result which wrongly indicates that the pathogen is present when it is not.¹³

Polymerase chain reaction is less time consuming as it takes an estimated 5 – 24 hours to produce a detection result. However, this method is very expensive and complicated and is reliant on a qualified professional to carry out testing. ^{2,3,13}

1.2.3: Immunological based detection

Some of the current immunological based detection techniques are enzyme immunoassay (EIA), enzyme linked immunosorbent assay (ELISA), enzyme linked fluorescent assay (ELFA). ELISA is a successful biosensor used to detect a wide range of pathogenic bacteria, toxins, fungi and mycotoxins. ^{2,13}

This method again requires highly qualified personnel, consumes a lot of time², and is particularly laborious. ¹

Table 1: Advantages and disadvantages of the current methods: Culture and colony, Polymerase chain reaction, immunological based detection

Type	Advantages	Disadvantages	References
Culture and colony	Most reliable and accurate, as well as the oldest technique	Experiment times for growing bacteria takes too long	4, 12, 13,
Polymerase chain reaction (PCR)	Very sensitive therefore small amounts of starting material can be used	Setting up and running requires great technical skill High equipment cost Highly sterile environment should be used to prevent DNA contamination	2, 3, 4, 12, 13
Immunological based detection	Very sensitive and specific sensor which can target explicit genes	Method requires highly qualified personnel Consumes a lot of time Well known as one of the more laborious methods	1, 2, 12

1.3: Electrochemical sensing

Electrochemical biosensors are a popular type of frequently used biosensor, ⁶ which are sufficient in detecting pathogens and their toxins. ¹³ This type of sensing is based on electrochemical species, such as electrons being consumed or produced, generating an electrochemical signal which can then be measured by an electrochemical detector. ^{6,15}

Some electrochemical biosensors are indirect in their detection and therefore rely on the detection of secondary tagged molecules. This method allows toxins with low molecular weights to be detected.¹³ Electrochemical methods such as amperometric, potentiometric and conductometric detection show promise as they overcome previously mentioned limitations, being low cost and useable for portable applications.¹⁶

1.3.1: Potentiometric sensors

Potentiometric devices measure the accumulation of a charge potential at the working electrode in comparison with the reference electrode, therefore providing information about ion activity in an electrochemical reaction. They function under equilibrium conditions and monitor the charge at zero current, created by selective binding at the electrode surface.

6,17,18

For potentiometric measurements, the relationship between the concentration and the potential is governed by the Nernst equation, where E_{cell} represents the observed cell potential at zero current. This can also be referred to as the electromotive force or EMF. E° cell is a constant potential contribution to the cell, R the universal gas constant, T the absolute temperature in degrees Kelvin, n is the charge number of the electrode reaction, F is the Faraday constant and Q is the ratio of ion concentration at the anode to ion concentration at the cathode.¹⁹⁻²¹

$$EMF \text{ or } E_{cell} = E_{cell}^{\circ} - \frac{RT}{nF} \ln(Q) \quad [\text{Equation 1}]$$

The direct determination of the analyte ion concentration with the Nernst equation is referred to as direct potentiometry.²² Low detection limits for potentiometric devices are currently often achieved with ion-selective electrodes (ISE). Therefore, by definition the detection limit is analyte specific and current devices are limited to detection between a range of 10^{-8} to 10^{-11} M. As potentiometric sensors ideally offer the benefit of not chemically influencing a sample, they are a good fit for measuring low concentrations in tiny sample volumes. The variety of ions, for which low detection limits are possible, is currently quite limited and missing important analytes, such as nickel, manganese, mercury and arsenate ions.^{20,22}

The sensors can also consist of biological structures, which can selectively adsorb microbes, coupled to an enzymatic transduction system. The enzyme-catalysed reaction only happens when a specific bacteria is adsorbed, which either creates or consumes a species which is

detected by the ion-selective electrode. This method gives high sensitivity, is time effective as well as economical. ^{9,23}

1.3.2: Amperometric sensors

Amperometric sensors are a type of electrochemical sensor, which measures current resulting from the oxidation or reduction of an electroactive species in a biochemical reaction.^{17,24} These methods are linearly dependant on analyte concentration and produce a normal dynamic range and a response to errors in the measurement of current. ⁶ In particular, these electrochemical biosensors are based on mediated or unmediated electrochemistry for electron transfer (Fig. 1).

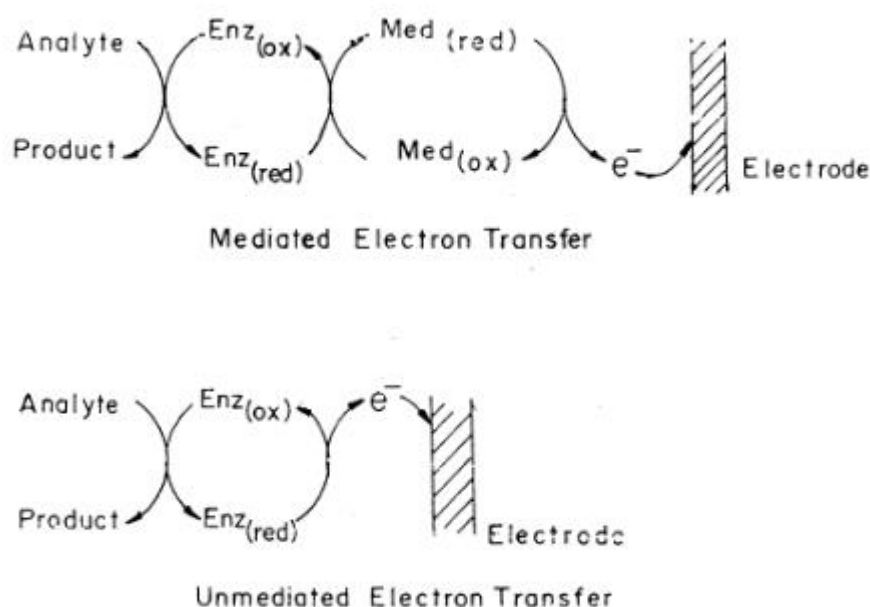


Figure 1: Scheme of mediated and unmediated electron transfer ⁶

The most commonly used mediators in mediated biosensors are ferrocene and its derivatives, ferricyanide, methylene blue, benzoquinone and N-methyl phenazine.⁶

1.3.3: Conductometric sensors

Conductometric biosensors measure the changes in the conductance between a pair of metal electrodes because of a biological component. ⁶ In most cases, conductometric

devices are used to study enzymatic reactions that produce changes in the concentration of charged species in a solution. The introduction of conductance biosensing and conductive polymer-based devices have been possible due to rapid development of semiconductor technology and sensor integration with microelectronic devices.¹⁷ Although conductometric sensing is not as popular as other sensing methods, there has been successful development of such devices in practical applications such as drug delivery in human urine and pollutant detection in environmental testing.^{17,25}

1.4. Nanoparticles and their physical and chemical properties

Nanoparticles are particles that are very small materials, ranging in size from 1 to 100nm. They spark wide scientific curiosity for many reasons, some which will be subsequently mentioned. They possess unique physical and chemical properties due to their high surface area and nanoscale size.^{26,27} As the physical properties of nanoparticles are quite different to those of bulk materials, this means that they can be used in a variety of new applications.

Some metallic nanoparticles have optical properties dependent on size, which allows them to appear as different colours due to their absorption in the visible region. These special optical properties occur due to the excitation of surface plasmons in a few metallic nanoparticles and can be used in biomedicine, energy and environment protection technologies.²⁸ The reactivity, toughness and other properties of these few metallic nanoparticles are also dependant on their unique size, shape and structure. These characteristics allow nanoparticles to be suitable candidates for various commercial and domestic applications, which include catalysis, imaging, medical application, energy-based research and environmental applications.^{26,29–33}

Nanoparticles are complex molecules, and consist of three layers. The first layer is the outer surface layer, which can be functionalised with a range of different small molecules, metal ions, surfactants and polymers. The shell layer makes up the second layer, which inherits a chemically different material from the core. This leaves the core as the third layer, which in essence is the centre of the nanoparticle.²⁶

1.4.1 Sensing of Bacterial pathogens

Advancements in nanotechnology, and surface functionalization of nanomaterials by biomolecule have led to new detections using nanobiosensors.^{1,11} Basic functions of

nanoparticles, catalysis of electrochemical reactions and the enhancement of electron transfer, make them very useful in designing novel electrochemical sensing systems.²⁸

The focus on detection, not of bacterial pathogens but their corresponding toxins, is currently a progressing area of interest.⁸ Pathogen detection and toxin detection differs largely due to the difference in size of each corresponding organism.¹³ To combat this issue, nanosensors are being developed in order to help detect smaller sized toxins and pathogens. Due to an enhanced detection limit, nanosensors, nanoelectrodes and many nanodevices are being more frequently used and developed for the detection of pathogens.³⁴

1.4.2: Gold nanoparticles as electrochemical biosensors

Functionalities can be added to nanomaterials by adding specific ligands to show changes in scattering and absorption of light in the visible region due to surface plasmon resonances. Colloidal metal nanoparticles such as gold, have different colours in solution due to their different surface plasmon resonances.³⁵ Their stability, self-assembly behaviour and mutual interactions of nanoparticles are very relevant to many colloid applications.²⁸

The versatility of gold makes them desirable materials for a range of biomedical applications. The alteration of physiochemical properties of gold nanoparticles such as surface plasmon resonance, conductivity and redox behaviour lead to detectable signals. Gold nanoparticles (AuNPs) also serve as practical platforms for therapeutic agents with their high surface area, allowing a dense presentation of multifunctional moieties.³⁶

Spherical gold nanoparticles, as mentioned previously, exert a range of colours, for example, brown, orange, red and purple, and show a size-relative absorption peak from 500 to 550nm. The absorption band arises from the collective oscillation of the conduction of electrons due to the resonant excitation by incident photons, (seen in Figure 2) which is called a surface plasmon band. This is influenced by not only size, but also shape, solvent, surface ligand, core charge, temperature and is even sensitive to the proximity of other nanoparticles. The aggregation of nanoparticles results in significant red-shifting of SPR frequency, broadening of surface plasmon band, which therefore changes the solution colour from red to blue due to the interparticle plasmon coupling.³⁶

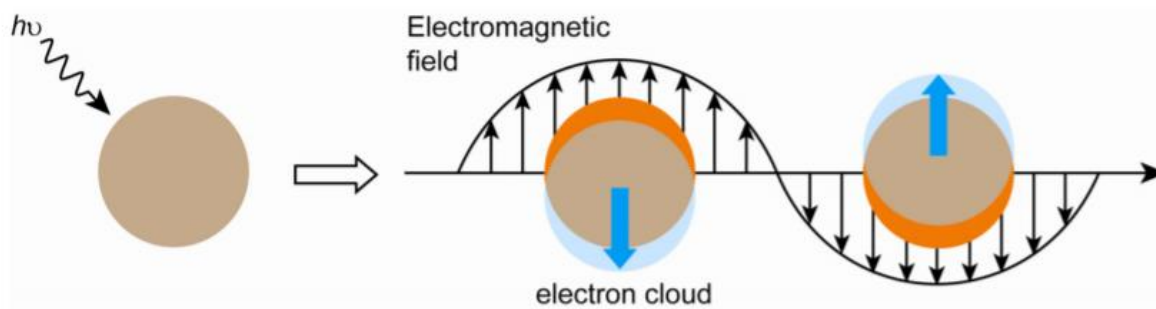


Figure 2: Schematic representation of the oscillation of conduction electrons across the nanoparticle in the electromagnetic field of the incident light

To conclude, the size-dependant optical properties of gold nanoparticles, along with the manipulation of thiols on their surface, are the main reasons to why AuNPs are being used in many biomedical applications, such as identifying toxins secreted by waterborne pathogens.¹

1.5: Previous synthesis methods of gold nanoparticles

Techniques for preparing gold nanoparticles can be categorized by two principles, the 'bottom up' or the 'top down' methods. The bottom up method includes chemical, photochemical and electrochemical techniques. These methods involve the assembly of atoms into desired nanostructures. A few popular top down methods, also described as physical methods, are photolithography and electron beam lithography, which require the removal of matter from the bulk material to get the desired nanostructure. Each methods can generate nanoparticles of different shape and size, but each having its own drawbacks, for example poor mono-disparity in bottom-up methods and extensive waste materials in top-down methods.³⁷

1.5.1: Physical methods

1.5.1.1: Electron beam lithography

EBL (Electron Beam Lithography) is a physical, lithographic technique for synthesizing metal nanoparticles.³⁸

The EBL method was mainly developed for manufacturing integrated circuits and leads to the formation of low dimensional structures in the resist, which can then be transferred into the substrate material via etching. This common technique generates metallic nanoparticles

which are controlled in size, shape and spatial distribution. The synthesis, as seen in Figure 3, is achieved by EBL through coating a substrate, such as a glass slide, with an electron sensitive resist, such as polymethyl methacrylate. The electron beam dissociates such coated substrate into fragments, which can be selectively removed with a chemical developing agent. The remaining nanoscale structure is suitable for the deposition of gold in the pattern formed by thermal evaporation, thus keeping the desired gold nanoparticle arrays on the glass slide.³⁹

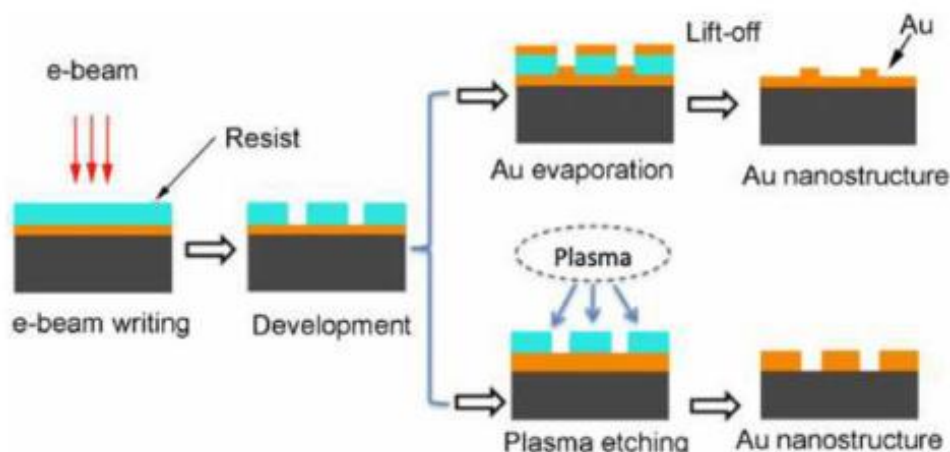


Figure 3: Schematic illustrating for the preparation method of Gold Nanoparticles using EBL. Ref. [39]

The main advantage of using EBL over other synthesis methods is its precise control of size, shape and spatial distribution of the nanoparticles formed.^{38,40}

Conversely, nanoparticles prepared via the EBL technique are limited to a working zone of a few hundred square microns and by separation distances between nanoparticles reaching a lower limit due to the size of the electron beam. As nanoparticles are not all geometrically 'perfect', i.e. spherical or ellipsoidal, these nanometric defects can lead to attenuation of the plasmon resonance and a broadening of the resonance peak.⁴¹ Other disadvantages of EBL include that it is known to be expensive due to the cost of e-beam writing systems, it generates low yields, and is a very time consuming process.^{38,40}

1.5.1.2: Photolithography

Photolithography is another top-down method, which involves the removal of matter from the bulk material to acquire a metallic nanostructure. Figure 4 shows a schematic diagram showing the process used to create nanoparticles via photolithography.⁴²

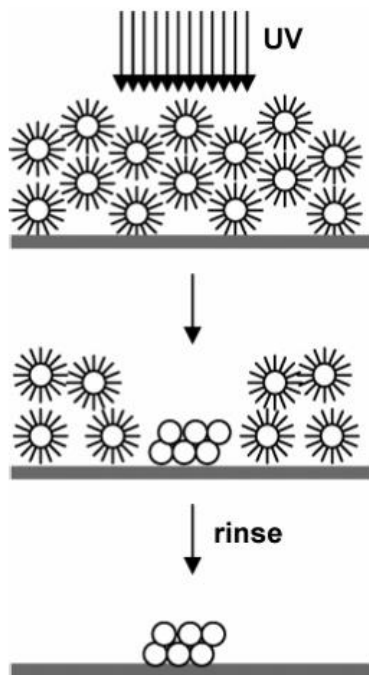


Figure 4: Schematic diagram showing the process used to generate nanoparticles. Aggregation of gold nanoparticles is achieved by the incident UV irradiation, leaving the final coagulated gold nanoparticles by washing away any left unirradiated particles. Ref. [29]

This technique requires an ultraviolet light (UV) which can be collimated through a quartz plane in order to create patterns on a surface. The light can transfer the desired pattern from the quartz plate, that serves as a mask, into an organic light sensitive material called photoresist. This can be then be coated on semiconductor substrates or wafers. ^{39,43}

Photolithography, like EBL method can create gold nanoparticles of particular size and shape, but they have their drawbacks, including having poor monodispersity as well as generating extensive waste materials when undergoing the process. ³⁷

1.5.2: Chemical methods

1.5.2.1: The Turkevich method

The Turkevich method was first coined in 1951 and is one of the most commonly used methods for synthesis for spherical gold nanoparticles. The principle of the method involves reduction of gold Au^{3+} ions to gold atoms Au^0 in the presence of reducing agents, such as citrate, amino acids, ascorbic acids or UV light. The size of the gold nanoparticles is then stabilized by various capping agents. ^{37,42,44–46}

1.5.2.2: The Brust Method

The Brust method originated in 1994.⁴⁷ This method is a two phase process which generates 1.5 – 5.2nm gold nanoparticles using organic solvents by varying the ratio of thiol to gold. The Brust method was inspired from Faraday's two-phase system. The method involves transfer of gold salt from aqueous solution to an organic solvent using a phase transfer agent. The reaction consists of a chlorauric acid solution with tetraoctylammonium bromide (TOAB) solution in toluene and sodium borohydride as an anti-coagulant, accompanied by a reducing agent. The gold is then reduced using sodium borohydride in presence of an alkane thiol. The alkane thiols stabilise the gold nanoparticles resulting in a colour change of the reaction from orange to brown.^{37,42,44,48}

1.5.2.3: Seeded growth method

A common method for the synthesis of gold nanoparticles is the seeded growth method. In this method, gold nanoparticles ranging from 5 – 40 nm diameter are synthesized. This method has an advantage of being a simple, quick and a low cost process.⁴²

The most common and widely used method is the seeded growth method. The basic principle of this technique is to first produce seed particles by reducing gold salts with a strong reducing agent like sodium borohydride. The seed particles are then added to a solution of metal salt in the presence of a weak reducing agent, as well as a structure directing agent to prevent further nucleation, and accelerate the anisotropic growth of gold nanoparticles. The geometry of the gold nanoparticles can be manipulated by varying the concentration of the seeds, reducing agents and structure directing agents.^{37,42,49,50}

In this project, this is the method to prepare the nanoparticles as described in Chapter 2.

1.6 Conclusion

It is evident electrochemical biosensors are commonly used for detection of species. These biosensors are based upon electrochemical species, such as electrons, which are consumed or generated during a bio-interaction process. This produces an electrochemical signal, which can be measured by an electrochemical detector.⁶

Characteristics mentioned previously, such as low cost, ease of use, portability and simplicity of construction, are the very reason why electrochemical methods are more

advantageous than the traditional methods mentioned in section 1.2. Additionally, as electrochemical biosensors adopt a surface technique, the method also allows very small sample volumes to be used for measurement.⁵¹ For these reasons, we have chosen to prepare an electrochemical biosensor.

Gold nanoparticles have many useful properties, including size and shape related optoelectronic properties, large surface-to-volume ratio, excellent biocompatibility and low toxicity. These are the main characteristics which make gold nanoparticles an important material in bionanotechnology.³⁶

This project aims to explore the use of modified nanoparticles in anticipation of creating a biosensor. This section has discussed and compared the different sensing methods and materials currently and previously used. It also touches upon the basic physical and chemical concepts of nanoparticles. It also explains how their characteristics make them advantageous when incorporated in electrochemical biosensing, as well as looking into the different synthesis methods used to create them. The next chapter will discuss the synthesis method chosen to produce gold nanoparticles, as well as how they are characterised later on.

Chapter 2:

Synthesis, growth and characterisation of Gold Nanoparticles

2.1: Introduction

Gold nanoparticles have many physical and chemical properties which make them excellent candidates for use in an electrochemical biosensor. The findings from previous syntheses of gold nanoparticles, as discussed in literature referenced in Chapter 1, also reinforce their suitability. This chapter will describe the synthesis which was followed and describe which characterisation methods were used to confirm the gold nanoparticles were successfully prepared, as well as concluding with a summary and an outlook.

2.2: Experimental approach

2.2.1: Synthesis of Gold Nanoparticles

Gold nanoparticles were prepared by the seed mediated method described by the procedure defined by Sau and Murphy.^{52,53}

The synthesis of gold nanoparticles starts with the preparation of the gold (Au^{3+} solution (A) as seen in as in Figure 5). To prepare this solution, $\text{HAuCl}_4 \cdot 3\text{H}_2\text{O}$ was dried in the oven (at approximately 70°C) to remove the excess of water as the salt is hygroscopic. The yellow, oven dried chloroauric acid, HAuCl_4 , was added to colourless cetyltrimethylammonium bromide, also known as CTAB (B), which were mixed homogeneously together upon addition. The solution was left to mix in a water bath which was set at approximately $25 - 30^\circ\text{C}$. This part of the synthesis was carried out at a specific temperature as CTAB in solution crystallises if the temperatures falls below 25°C . The mixture of two reagents produced a light yellow / orange solution. The new solution (C) was then left to mix in the water bath for 30 – 45 minutes. Next, sodium borohydride, NaBH_4 was added to the yellow / orange solution. The preparation of 0.01 M NaBH_4 solution was carried out in an ice-cold environment to prevent the NaBH_4 from decomposing. Upon addition of the NaBH_4 the solution turned into a dark brown solution (G).

Lastly the reaction was left to mix for approximately 2 hours inside a water bath at 25°C.

The solution turned from a brown solution (G) into a wine-red solution (H). This colour change was seen as a result of letting the reaction mix, where the gold nanoparticles were allowed to grow to their desired size.

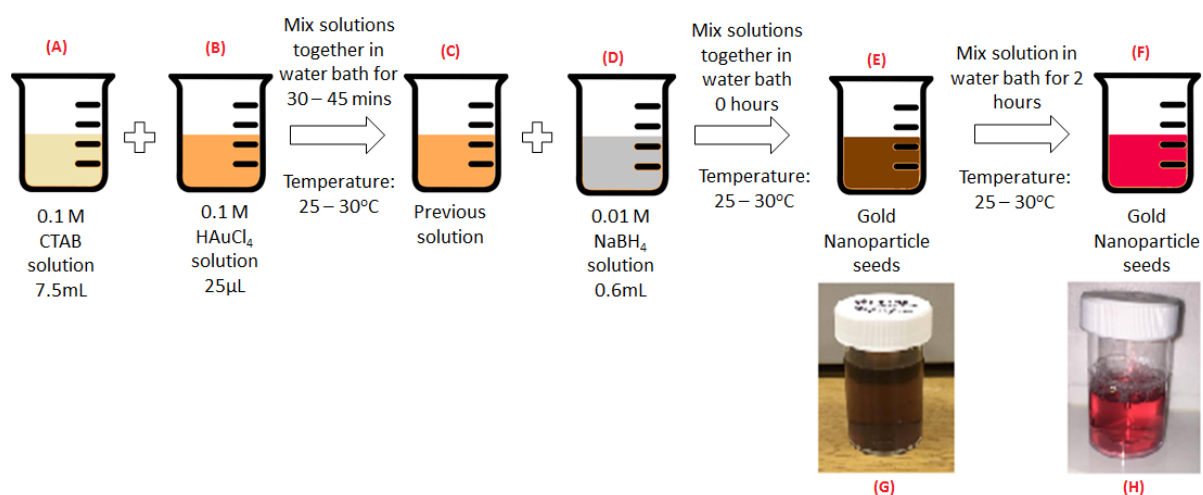


Figure 5: Schematic diagram of the synthesis of gold nanoparticles.

During the procedure there was difficulty in controlling the nucleation and growth steps which occurred at the intermediate stages of particle formation. This led to broad results of particle size distribution. Growth of the colloidal gold nanoparticles is induced by the presence of cationic CTAB. The $AuCl_4^-$ ions are bound to CTAB micelles, which are electrostatically repelled from the CTAB capped gold nanoparticles. The growth of gold nanoparticles is controlled by CTAB. ⁵⁴



This reaction occurs at nanoparticle surface sites, showing the procedure of the narrowing of the nanoparticle size shape and distribution.

2.2.2: Chemical cleaning method of Gold Nanoparticles

After the gold nanoparticles were synthesised, the following protocol was used for cleaning the nanoparticles and removal of the excess of surfactant. To remove the excess reactants in the solution the gold nanoparticles were centrifuged three times at 4000 rpm during 30 minutes in ultrapure water as described in reference ⁹. NaOH pellets were then added to the cleaned gold nanoparticles to destabilize the CTAB adsorbed on the surface of the gold

nanoparticles, inducing the precipitation of CTAB. After this step, the gold nanoparticles were cleaned another time before being collected, leaving behind and discarding the resulting supernatant.

This procedure of centrifuging and re-dispersion in ultrapure water allows the removal of CTAB, as well as NaOH, from the surface of the particles.

2.3: Principles of characterisation of Gold Nanoparticles

2.3.1: Characterisation by UV-Vis

Nanoparticles have optical properties which are very sensitive to size, shape, agglomeration and concentration changes. UV-Vis measures the intensity of light that is passing through the sample, which allows the estimation of size, shape, and aggregation level of metal nanoparticles.^{27,55,56} The nanoparticles also obtain optical properties as a consequence of collective oscillations of conduction electrons, which is excited by electromagnetic radiation called surface plasmon polariton resonances (SPPR). Those changes have an influence on the refractive index next to the nanoparticles surface, therefore, making it possible to characterize nanomaterials using UV-Vis. ⁵⁶

The extinction spectra of AuNP recorded by UV-Vis spectroscopy can be analysed using Mie Theory. ⁵⁷⁻⁵⁹ However, this is dependent on the appropriate correction of metal dielectric constant for the nanoparticle size, and the physiochemical environment as shown by direct measurements on single nanoparticles.

The Plasmon resonance is also affected by the multiple factors mentioned previously, including environment dielectric properties, physical or chemical interactions on particles surface, surface charge, interparticle distance and aggregation. ⁶⁰

All UV-Vis characterisation of the gold nanoparticles was carried out on a Cary50 UV-Vis Spectrophotometer. Using the data collected we can determine the wavelength and absorption where the SPR peak occurs. Figure 6 shows the UV-Vis spectra of the gold nanoparticles which were synthesized. The position of the peak is related to the particle diameter, while the absorbance provides information on the concentration of the gold nanoparticles.⁶¹ The gold nanoparticle wavelength peak is at 527nm, which corresponds to the gold nanoparticles being ~30nm in size.

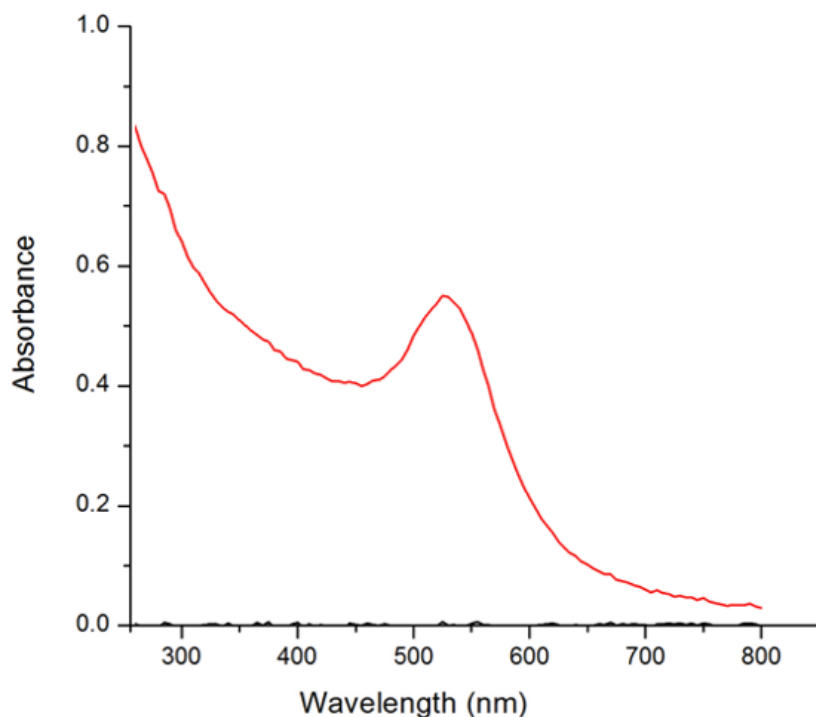


Figure 6: UV-Vis Spectra of Gold Nanoparticles carried out on a Cary50 UV-Vis spectrophotometer. Peak for nanoparticles occur at 527nm.

Size and concentration of the gold nanoparticles can be determined directly from UV-Vis spectra using the equations below.

In order to calculate the concentration of gold nanoparticles in solution, we can refer to Beer Lamberts Law, ⁶¹

$$A = \epsilon c l \quad \text{[Equation 3]}$$

Where the product of molar concentration (c), molar absorptivity (ϵ) and the path length (l) equals to the absorbance. ⁶²

During the procedure, two attenuating species will occur in solution (sodium borohydride and gold ³⁺).

In order to determine the diameter of gold nanoparticle (d) can be represented as:

$$d = e^{\frac{A_{spr}}{A_{450}} B_2} \quad \text{[Equation 4]}$$

By knowing the absorbance at the SPR (surface plasmon resonance) peak and 450nm, we can estimate that the gold nanoparticles will measure between 5nm and 80nm. Variables B_1

and B_2 are experimentally calculated values.⁶³ They are dependent on the ratio of A_{spr} / A_{450} . As previously mentioned, A_{spr} is the absorbance at SPR whilst A_{450} is the lowest absorbance close to the peak at 450nm.

2.3.2: Characterisation by X-Ray Diffraction

X-ray diffraction (XRD) patterns were obtained with a Bruker AXS D2 PHASER diffractometer by using $\text{CoK}\alpha$ (0.179 nm) radiation. Samples were prepared by depositing drops (20 μL) of the CTAB- protected nanoparticles on a quartz holder and drying in air.⁵²

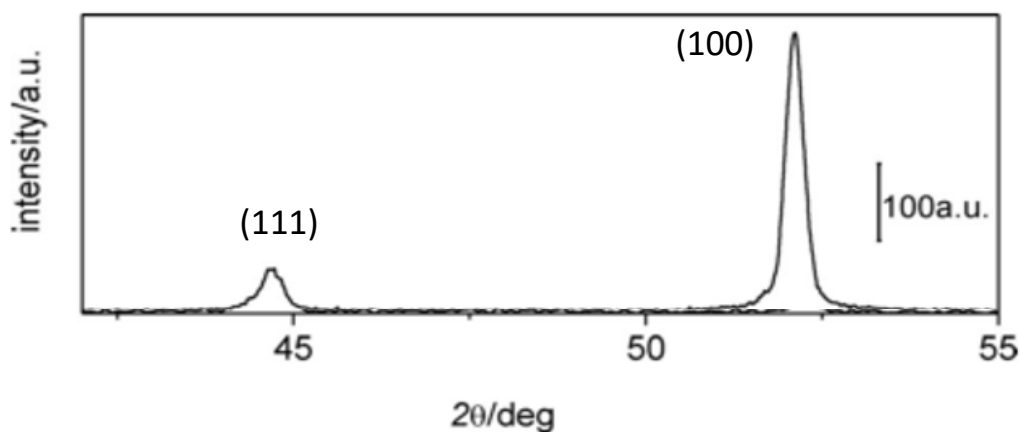


Figure 7: XRD patterns of corresponding (A) Au cubic nanoparticles.

Figure 7 shows the XRD of cubic nanoparticles, which suggest the presence of (100) facets. The XRD patterns are due to relative intensity of diffraction peaks indicating the presence of preferential orientation.^{52,64}

Furthermore, the large $[\text{RNMe}_3]^+$ head-group of CTAB (rough diameter = 0.814 nm, area = 0.521 nm^2) and the long alkyl chain are more readily accommodated on the (100) side edges, than on close-packed (111) faces, where the Au–Au spacing is too small to facilitate epitaxy.⁶⁴

2.3.3: Characterisation by Transmission Electron Microscopy

Transmission electron microscopy was performed by using a JEOL JEM 1200 EX MKI instrument. Samples were prepared by drop-casting the ethanolic suspensions of each catalyst on carbon coated copper grids and drying in air.⁵²

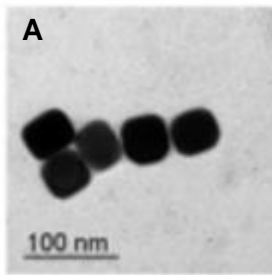


Figure 8: TEM images of (A) Au cubic nanoparticles.

Figure 8 shows the TEM images above from Monzo et al., 2015 and indicates the presence of 45 – 50 nm particle sized gold cubes.⁵²

2.4 Conclusions

The characterisation methods above show the synthesis followed did result in producing gold nanoparticles. Au nanoparticles are commonly known to show strong surface plasmon resonance (SPR) that is dependent on their size and shape. Spherical AuNPs, as referenced from the literature, can show an absorption band anywhere in-between 515 – 572nm, with the position depending on the diameter of the gold nanoparticles. The UV-Vis spectra of the particles in Figure 6 show that the position of the SPR peak is 527nm, therefore the gold nanoparticles are 30nm in size.

Chapter 3: Electrochemical Cleaning and Characterisation of Gold Nanoparticles

3.1: Fundamentals of Electrochemical Characterisation by Cyclic Voltammetry

After physical characterisation, the gold nanoparticles were characterised electrochemically.

Electrochemical characterisation incorporates the study of chemical response, in particular the gain or loss of electrons in a system, as a response to an electrical stimulus.

Electrochemical experiments involve the measurement of one of four parameters being: current, time, charge and potential. The technique used in this case was cyclic voltammetry (CV).⁶⁵

3.1.1: What is Cyclic Voltammetry

Electrochemistry techniques link the flow of electrons to chemical changes, a method which is commonly used to characterise an electrode's surface. This common and powerful electrochemical technique does this by investigating the reduction and oxidation processes of a molecular species.

Electrons are tiny and have a very small charge. A large amount of electrons can be defined as 1 unit of charge, called a coulomb. One coulomb is equivalent of 6.2×10^{18} electrons. The rate of coulombs flowing in a circuit (the number of coulombs per second), is called the current. The energy of a coulomb is called the voltage and is measured in joules.

To deduce the amount of electrical charge that flows in a circuit, the following equation is used:^{66,67}

$$C = A \times T \quad \text{[Equation 5]}$$

Where:

C = Charge

A = Current

t = Time

If the electrical charge and the voltage (also referred to as the potential difference) is known, then the energy transferred during a reaction can be found by:

$$J = V \times C \quad \text{[Equation 6]}$$

Where:

J = Energy transformed

V = Potential difference

C = Charge

The dependence on whether two electrical charges repel or attract each other depends on each particles' charge in coulombs and the distance between the two particles. If the polarities are the same, then the coulomb force repels, but if the polarities are opposite the coulomb force attracts. The electrical charge is inversely proportional to the square of the separation distance between the two particles. This is described as Coulombs law, which is:

$$F = \frac{kq_1q_2}{r^2} \quad \text{[Equation 7]}$$

Where:

F = Electric force

(q₁) = Charge 1

(q₂) = Charge 2

r = Distance between (q₁) and (q₂)

k = Coulomb's constant

A CV scan is obtained by cycling the potential of an electrode, which is immersed in an unstirred solution and measuring the resulting current at the working electrode. The current can be considered the response signal to the potential excitation signal. The CV is a display of the current (vertical axis) versus potential (horizontal axis). As the potential varies linearly with time, the horizontal axis can also be thought of as a time axis.

The potential of the working electrode is controlled against a reference electrode. The controlling potential which is applied across two electrodes can be considered an excitation signal. The counter electrode, also known as the auxiliary electrode, is then used to close the current circuit in the electrochemical cell. The excitation signal for CV is a linear potential

scan with a triangular wave form. It can be seen in the figure below. The potential excitation signal sweeps the potential of the electrode between two values, and is sometimes called the switching potentials. In Figure 9, the scans are between 0.8 and -0.2 V. ^{68,69}

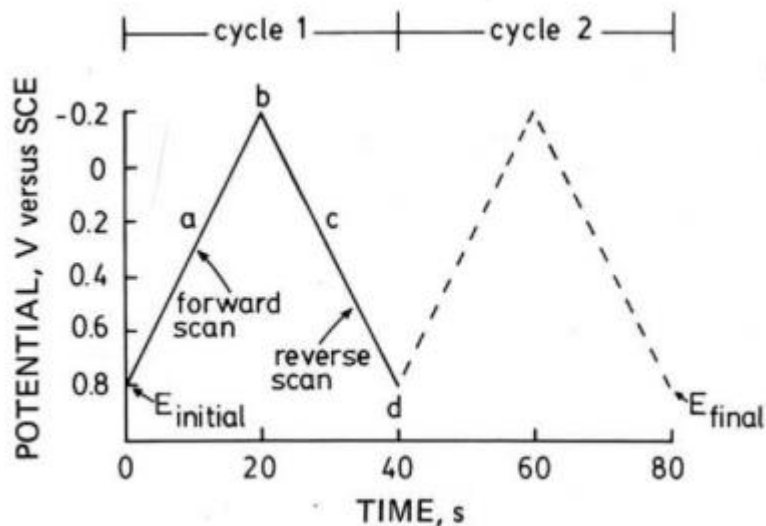


Figure 9: Typical excitation signal for cyclic voltammetry—a triangular potential waveform with switching potentials at 0.8 and -0.2 V versus SCE. Ref. ⁶⁹

The scan rate of the experiment controls how fast the applied potential is scanned. The diffusion layer is decreased in size as a result of faster scan rates. Therefore, in these instances, higher currents are observed. ⁶⁸

The maths which determines a cyclic voltammetry is challenging, however Fick's First Law of Diffusion explains that the current at any time, t , is proportional to the concentration gradient of the reactant, as described in the equation below: ⁷⁰

$$i_t = n F A D_0 (\partial C_0 / \partial x) x - Qj \quad \text{[Equation 8]}$$

Where:

i_t = Current (at any time)

n = Number of electrons

F = Faradays constant

A = Electrode area

D_0 = Diffusion coefficient

C_0 = Change in concentration of the particle

x = Distance from the electrode surface

Q = Charge

j = Flux Density

3.1.2: Reversible and Irreversible systems

The electron transfers kinetics between electrode and the analyte denote to determine whether a process is electrochemically reversible.⁶⁸ Electrochemically, reversible processes imply that the undergoing reactions are fast enough to maintain concentrations of oxidized and reduced forms in equilibrium with each other, at the electrode surface.

The ratio at a given potential is determined by the Nernst Equation: ^{68,70}

$$E = E^{o'} - \frac{RT}{nF} \ln \left(\frac{[Red]}{[Ox]} \right) \quad \text{[Equation 9]}$$

where:

$E^{o'}$ = Reduction potential

R = Gas Constant

T = Temperature

n = Number of electrons

F = Faradays constant

[Red] = Reduction

[Ox] = Oxidation

Normally, electrochemically reversible processes, where fast electron transfers occur, and those that follow the Nernst equation, are referent to as Nernstian. ⁶⁸

The magnitudes of anodic peak current i_{pa} , cathodic peak current i_{pc} and anodic peak potential E_{pc} are important parameters of CV. As a chemically reversible couple where a redox species rapidly exchanges electrons with the working electrode, we find that for a reversible couple, the formal reduction potential $E^{o'}$ is centred between E_{pa} and E_{pc} .

The formal reduction potential ($E^{o'}$) for a reversible process is centred between E_{pa} and E_{pc} .⁶⁹

$$E^{o'} = \frac{E_{pa} + E_{pc}}{2} \quad \text{[Equation 10]}$$

where:

E_{pa} = anodic peak potential

E_{pc} = cathodic peak potential

The number of electrons transferred in the electrode reaction (n) for a reversible process can be determined from the separation between peak potentials. ⁶⁹

$$\Delta E_p = E_{pa} - E_{pc} \cong \frac{0.059}{n} \quad \text{[Equation 11]}$$

For a reversible system, the peak current is defined by the Randles-Sevcik equation for the forward sweep of the first cycle.

$$i_p = (2.69 \times 10^5) n^{\frac{3}{2}} A D^{\frac{1}{2}} C v^{\frac{1}{2}} \quad \text{[Equation 12]}$$

where:

i_p = Peak current

n = Electron stoichiometry

A = Electrode area

D = Diffusion coefficient

C = Concentration

V = Scan rate

Consequently, i_p increases with square root of v and is directly proportional to concentration. The values of i_{pa} and i_{pc} should be identical for a simple reversible (fast) couple. That is: ^{68,69}

$$\frac{i_{pa}}{i_{pc}} = 1 \quad \text{[Equation 13]}$$

Alternatively, slow electron change of the redox species with the working electrode indicates electrochemical irreversibility. As previously mentioned, equations 10, 11, 12, and 13 are considered when both species in a redox couple rapidly exchange electrons; therefore for irreversible reactions, they are not applicable. Subsequently, electrochemical irreversibility is defined by separation of peak potentials greater than indicated in equation 10. ⁶⁹

Deviations from the linearity plots of i_p vs $v^{1/2}$ mentioned above, is presumed to be for analytes which are to be freely diffusing species. These processes are either suggesting electrochemical quasi-reversibility or that the electron transfer may be occurring via surface adsorbed species. Analysing the peak to peak separation can help differentiate between the two causes of deviation. Electrochemically, quasi-reversible processes have the peak to peak separation shifts with scan rate. Whereas, in the surface adsorbed species, no peak to peak separation is witnessed. ^{68,70}

3.2: Electrochemical set-up

Cleaning procedures for the glassware used are carried out daily to help produce reproducible experimental conditions. All glassware used, including the electrochemical cells, were soaked overnight in acidic K_2MnO_4 . The acidic K_2MnO_4 is used as it is a powerful oxidising agent, which helps remove any unwanted organic residues. The glassware is then carefully removed from the acidic $KMnO_4$ and rinsed with ultrapure water, followed by a diluted solution of hydrogen peroxide and sulfuric acid (3:1), also known as piranha solution, then rinsed again with ultrapure water.⁷¹ The piranha solution is used to remove any traces of manganese oxides which remain.⁷² Lastly, the electrochemical cell was assembled, filled 1/3 with ultrapure water and heated on a hot plate to remove the excess of sulphate from the cell. This process of boiling is repeated another 4 times, using fresh ultrapure water each time.

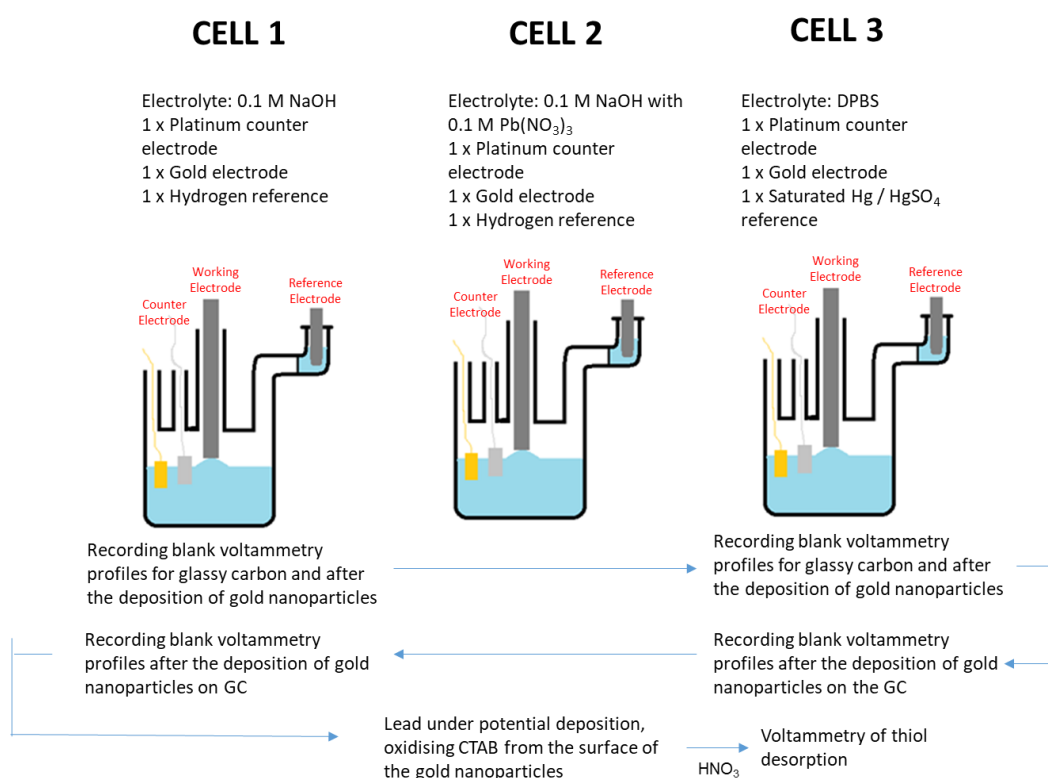


Figure 10 : Schematic diagram of the electrochemical experimental protocol. Further explanation can be found in the rest of section 3.2.

As seen in Figure 10, three electrochemical cells were used for the duration of the experiments. The two compartment electrochemical cells were connected to an μ Autolab III

potentiostat which conducted the electrochemical measurements. For each part of the experimental procedure, the same gold nanoparticle supported glassy carbon working electrode was used.

A saturated reference Hg/HgSO₄ electrode was used for the cell containing Dulbecco's Phosphate Buffer Saline (DPBS), whereas for the cells containing 0.1 M NaOH, the RHE reference was used. These two different reference electrodes were used as separate mediums to conduct the experiments. Gold and platinum counter electrodes, with an electrochemical surface area, are approximately 50 times bigger than the working electrode; which was used in the experiments described. All potentials in the cyclic voltammetry's performed were converted to RHE.

The potential provided by an RHE is given by the equation

$$E = E_0 - \left(\frac{RT}{nF}\right) \ln [H^+] \quad \text{[Equation 14]}$$

Where:

E_0 = Standard state cell potential

R = Gas Constant

T = Temperature

n = Number of electrons

F = Faradays constant

[H⁺] = Concentration of hydrogen ion

Each electrochemical cell was bubbled through with argon to deoxygenate all electrolytes. This process is carried out before the start of any experiment in order to remove any oxygen in the cell, which is redox active.

3.2.1: Cleaning of the Glassy Carbon electrode

Electrochemical measurements taken are very sensitive. Therefore, before conducting any experiments, the glassy carbon electrode must be cleaned to remove any contaminating molecules that may be present.

The glassy carbon electrode was hand polished with an alumina⁷³ slurry for 5 minutes. The working electrode was then immersed into a clean glass vial with ultrapure water, which was

left to sonicate for 5 minutes. After sonicating the working electrode was thoroughly washed with ultrapure water. Lastly, the working electrode was rinsed with ultrapure water to ensure that all excess alumina paste had been removed.

After this cleaning procedure, a blank CV of the GC was recorded to ensure there were no impurities from previous experiments, or excess of alumina on the glassy carbon electrode.

Figures 11A and 11B show the voltammetric profiles of the clean glassy carbon working electrode in 0.1 M NaOH and DPBS.

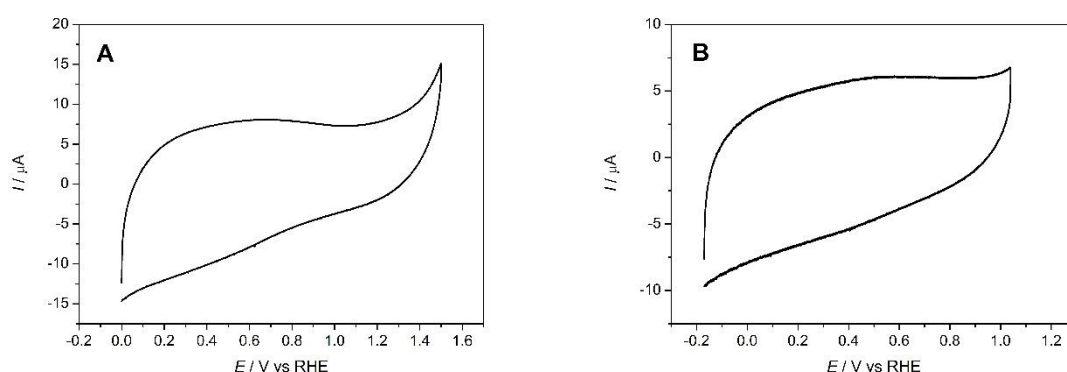


Figure 11: Voltammetric profiles of glassy carbon electrodes after cleaning procedure, A recorded in 0.1 M NaOH and B recorded in DPBS. Scan rate $\nu = 50 \text{ mV s}^{-1}$.

As demonstrated in figure 11, the absence of any redox peaks highlights the electro-inactive nature of glassy carbon in both a neutral A and alkaline B electrolyte.

Once the clean glassy carbon electrode was characterised, the thin film of gold nanoparticles was prepared as described in the following section.

3.2.2: Preparation of Gold Nanoparticle coated working electrode

Firstly, to ensure a homogeneous distribution of the gold nanoparticles in the solution, the nanoparticle suspension was sonicated for 5 minutes.

The clean glassy carbon working electrode blank cyclic voltammetry was washed with ultrapure water and then dried in an oven (approximately 60°C). Next the electrode was prepared by depositing different amounts of $1.5\mu\text{L}$ of gold nanoparticle droplets onto the working electrode via the drop cast method.⁷⁴ Each drop was allowed to fully dry before another one was added to increase the attachment to the GC, and to create a homogeneous

layer of the gold nanoparticles over the surface of the glassy carbon electrode. After the final drop was added and dried, the working electrode was again rinsed with ultrapure water before carrying out blank CVs.

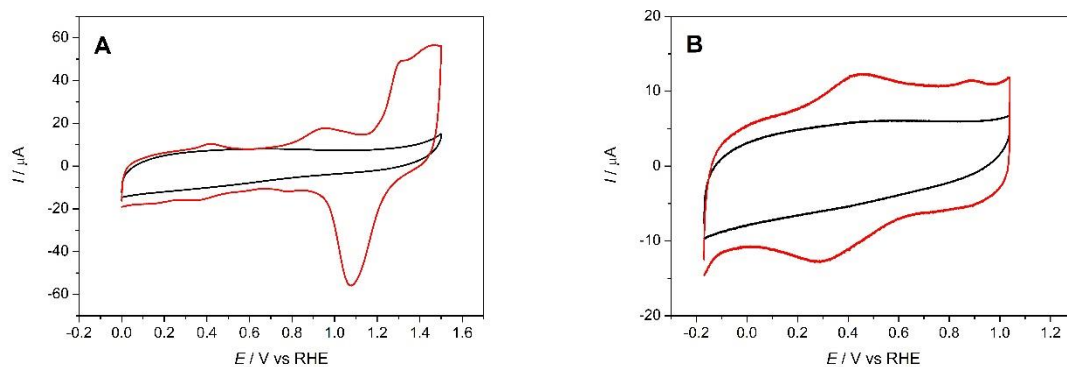


Figure 12: Voltammetric profiles of gold nanoparticle covered glassy carbon working electrode. Both profiles show the glassy carbon blank (black), and the gold nanoparticle scan (red). A recorded in 0.1 M NaOH and B recorded in DPBS. Scan rate $u = 50 \text{ mV s}^{-1}$.

Figures 12A and 12B above show the two cyclic voltammetry's comparing the glassy carbon and gold nanoparticle deposited working electrode CV. From both figures, it is evident that there is a clear change from before and after the deposition of gold nanoparticles. In figure 12A, the peak corresponds to the formation of gold oxides from $\text{Au} \rightarrow \text{AuO}_x$ when the working electrode scans at high potentials. In 12A, a peak at 1.0 shows that there are some unknown impurities which have been detected. At 1.1 V the gold reduction peak occurs where $\text{AuO}_x \rightarrow \text{Au}^0$.⁴⁶ In Figure 12B, the red scan shows small broad peaks which are approximately at 0.4 V and 0.8 V. These peaks correspond to the adsorption of anions in DPBS on the gold surface.⁴⁶

3.3: Electrochemical Cleaning and Characterisation of Gold Nanoparticles using Pb Under Potential Deposition

3.3.1: Cleaning of gold nanoparticles by Lead UPD

After the removal of excess CTAB and reactants from gold nanoparticles, by centrifuging and rinsing with water, the gold nanoparticles still have a substantial amount of CTAB on their surface. The aim of using lead under-potential deposition is to completely remove all

the CTAB present on the surface of the gold nanoparticles. To undergo this experimental procedure 0.1 M $\text{Pb}(\text{NO}_3)_2$ salt is added and allowed to dissolve in the 0.1 M NaOH electrolyte.

The process is achieved by depositing a layer of PbO_2 on the electrode surface at high potentials.³²

The gold nanoparticles are cycled at low potentials to remove any organic species on their surface by the oxidation of PbO_2 .³² The cyclic voltammetry in Figure 13A shows the potential region, 0.25 to 0.8 V vs RHE, whilst in Figure 13B this is 0.25 to 1.7 V vs RHE. The cyclic voltammeters obtained show profiles where lead has been oxidised and reduced on the surface of the gold nanoparticles, as well showing the different peaks appearing for the different surface orientations of the gold nanoparticles on the working electrode, which can be seen at 0.4 and 0.6 V vs RHE.^{52,74,75}

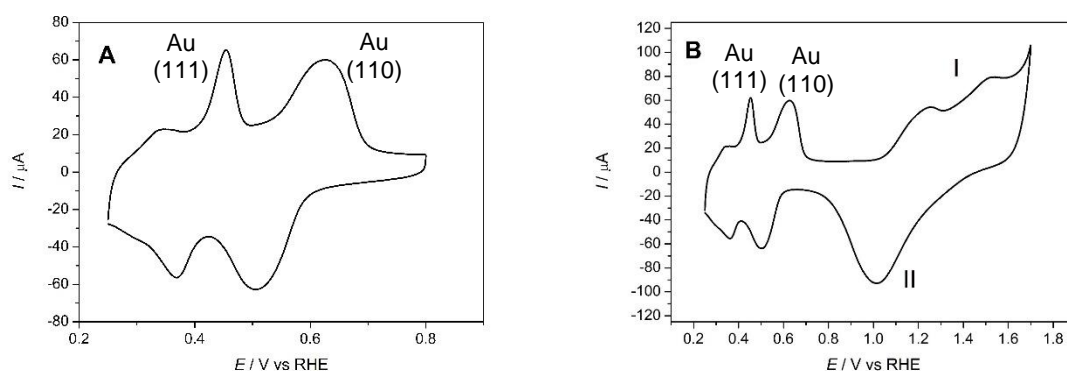


Figure 13: Voltammetric profiles of gold nanoparticle after the deposition / dissolution of the PbO_2 film, cycle between the potential ranges (A) 0.25 and 0.8 V and (B) 0.25 to 1.7 V. Both profiles recorded in 0.1 M NaOH and 0.1 M $\text{Pb}(\text{NO}_3)_2$. Scan rate $\nu = 50 \text{ mV s}^{-1}$.

In Figure 13B, there are broad peaks at high potentials (I) corresponding to lead oxidation and (II) corresponding to lead reduction.

In Figure 13A, gold nanoparticle CV peaks can be labelled to corresponding gold surface orientations. The three surface orientations which gold can possess are Au(111), Au(100) and Au(100), as can be also seen in Figure 14. In figure 13A, peaks at potentials 0.38 V and 0.5 V correspond to Au(111) and Au(110) surface orientations of the gold nanoparticles.⁷⁶

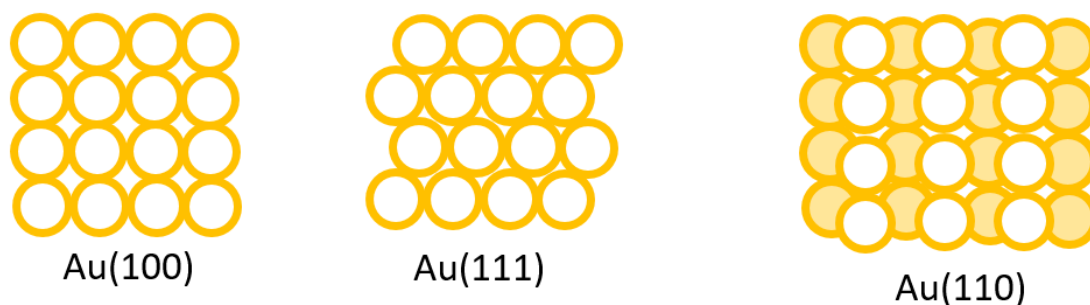


Figure 14: Surface orientations of Au(100), Au(111) and Au(110)

After the electrochemical cleaning process, 0.1 M HNO₃ was used to remove any remaining PbO₂ on the surface by dissolving the excess. The working electrode was dipped in 0.1 M HNO₃ twice for 5 minutes, before and after when the working electrode was rinsed.⁷⁵

Figure 15A and 15B show the comparison of CVs before and after the working electrode was cleaned with 0.1 M HNO₃. In figure 15A, the peaks for lead oxidation and reduction disappear after the cleaning procedure. In figure 15B, the peaks at approximately 0.4 and 0.9 V disappear as the excess lead is removed from the working electrode. The disappearance of the peaks in both Figures 15A and 15B correspond to the excess lead being removed from the surface of the clean gold nanoparticles.

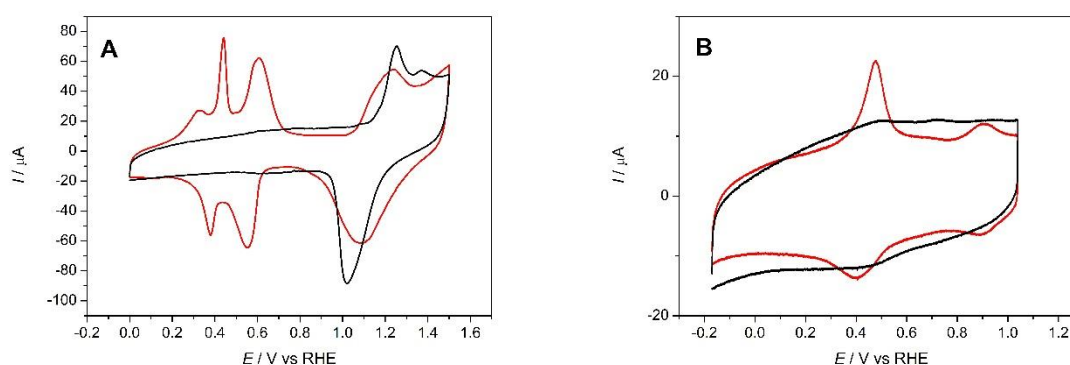


Figure 15: Voltammetric profiles of gold nanoparticle supported glassy carbon working electrode. Black scan shows the cleaned gold nanoparticles, red scan shows gold nanoparticles after immersing the working electrode in nitric acid, A recorded in 0.1M NaOH and B recorded in DPBS. Scan rate $u = 50 \text{ mV s}^{-1}$.

Figures 16A and 16B below show the comparison of the gold nanoparticle scans before and after the Pb UPD cleaning process. As a result, both scans in A and B after Pb UPD have a

higher charge, therefore showing increased peaks as a result of cleaning excess CTAB from the surface of the gold nanoparticles. Figure 16A shows the increased oxidation and reduction peaks of gold due to the changing of the surface orientations.

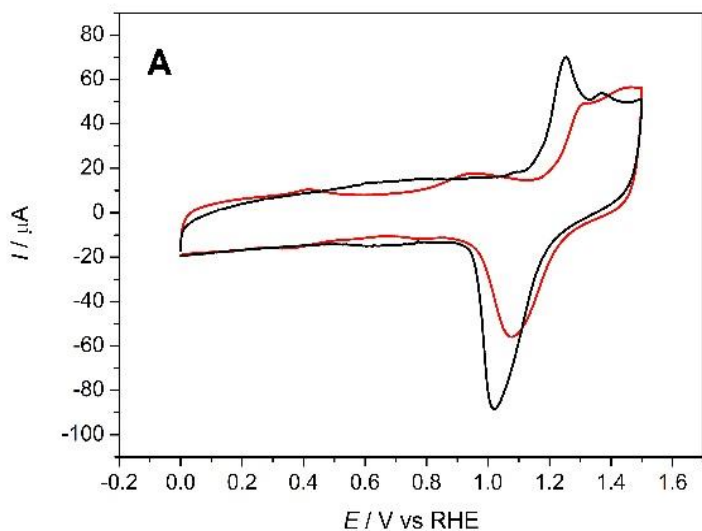


Figure 16A: Voltammetric profiles of gold nanoparticle covered glassy carbon working electrode. Red line is the gold nanoparticle blank after initial deposition of nanoparticles onto working electrode. The black line shows gold nanoparticle scan after Pb UPD cleaning process. A was recorded in 0.1M NaOH Scan rate $u = 50 \text{ mV s}^{-1}$.

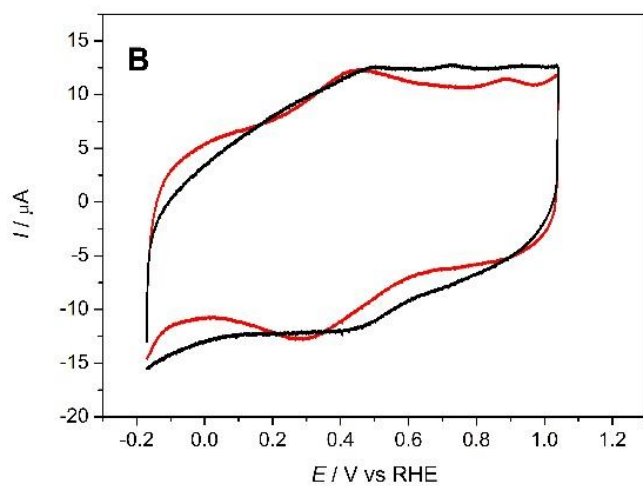


Figure 16B: Voltammetric profiles of gold nanoparticle covered glassy carbon working electrode. Black line is the gold nanoparticle blank after initial deposition of nanoparticles onto working electrode. The red line shows gold nanoparticle scan after Pb UPD cleaning process. B was recorded in DPBS. Scan rate $u = 50 \text{ mV s}^{-1}$.

The change in the peaks seen in both CV's before and after UPD is due to CTAB being oxidised from the surface of the gold nanoparticles. Therefore, gold oxidation and reduction

peaks increase, which are further depicted in Figures 16A and 16B. This change is witnessed mostly in Figure 16A, showing the increased signal of gold reduction, which is expected after CTAB is oxidised.

The reduction monolayer of gold oxide can be used to determine the electrochemical surface area of the gold nanoparticles on the electrode. The charge of the reduction of the monolayer for gold oxide on a poly-oriented electrode, when the anodic limit of the voltammogram is set just before the onset of oxygen evolution reaction is $420 \mu\text{C cm}^{-2}$. The electrochemical surface area from figure 16A was 0.0128cm^2 .^{52,76,77}

3.4: Conclusions

To conclude, by cleaning the gold nanoparticles via the method of Pb UPD it can be ascertained that the two CVs, including profiles of gold oxidation and reduction peaks, have increased in comparison to the scans before and after Pb UPD.

Another success from using this method is the removal of impurities upon the surface of the electrode, or on the surface of the gold nanoparticles. Figure 12A shows a scan of the gold nanoparticles with the impurities seen at 1.0 v vs RHE, which after Pb UPD have been removed in Figure 16A.

Therefore, the increased signal of gold oxidation and reduction in the CVs leads us to believe that a substantial amount of CTAB has been removed by undergoing this process.

Chapter 4: Electrochemical stability of modified gold electrodes

4.1: Introduction

Due to the discovery and widespread use of self-assembled monolayers adsorbed onto metal colloids, surface composition of gold nanoparticles can be modified to contain a range of functional groups.^{78–80}

The most stable thiol or disulphide is most desirable as the fundamental part of the sensor is the sulphur containing molecule. Chapter 4 discusses the electrochemical stability of modified gold nanoparticles by the sulphur containing molecules depicted below in Figure 17.

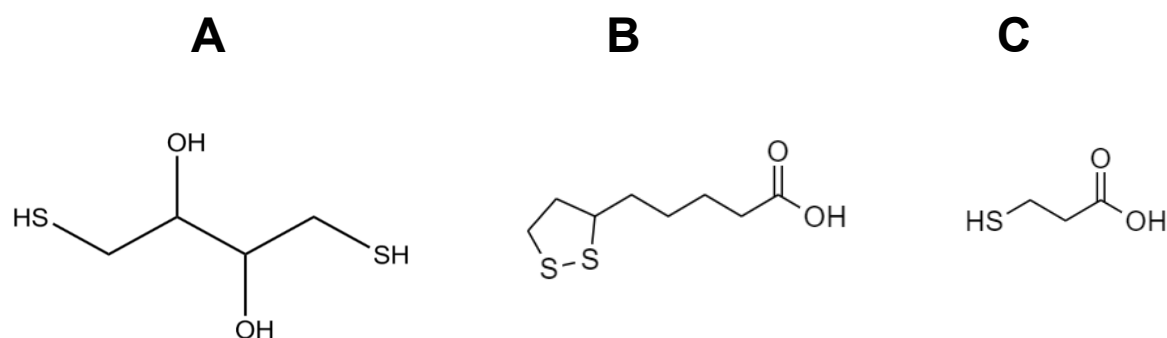


Figure 17: (A) 1,4-dithiothreitol, (B) thiocetic acid and (C) 3-mercaptopropionic acid.

4.1.1: The chemistry of 1,4-dithiothreitol

Dithiothreitol (DTT) is a common name for the small molecule redox reagent also known as Cleland's reagent. DTT's chemical formula is $C_4H_{10}O_2S_2$ and the chemical structure is shown below. DTT also has an epimeric resulting form when oxidised, known as dithioerythritol (DTE), as seen in Figure 18. DTT, and its isomer dithioerythritol, are widely used reagents for the reduction of disulphide bonds in proteins and other disulphides.

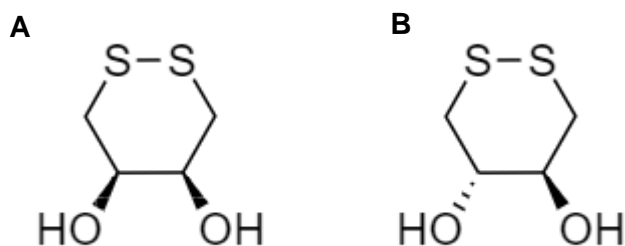


Figure 18: Figure (A) shows dithiothreitol (DTT) and (B) the oxidized form dithioerythritol (DTE)

The oxidation of DTT over time can be monitored by UV-Vis as seen in the literature.

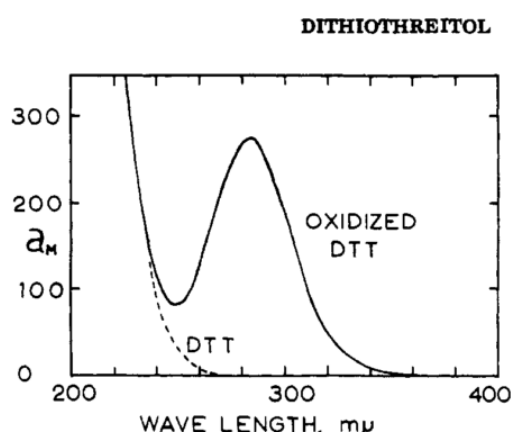


Figure 19: UV-Vis spectra of DTT in comparison with its oxidised form ⁸¹

4.2: Experimental procedure:

4.2.1: Surface modification of gold electrode using 1,4-dithiothreitol, thiocetic acid and 3-mercaptopropionic acid

The gold nanoparticle supported glassy carbon electrode was functionalised with self-assembled monolayers of three different sulphur-containing molecules.

Freshly prepared solutions of 0.1 M dithiothreitol in ultrapure water, 0.1 M thiocetic acid in ethanol and 0.1 M 3-mercaptopropionic acid in a solution of ethanol and ultrapure water (75:25) were used within the procedure. For the solution of 3-mercaptopropionic acid, the mixture of ethanol and ultrapure water is used so the 3-mercaptopropionic acid fully dissolved in the solution. ⁸²

After the solutions were prepared, the working electrode was cleaned with ultra-pure water in anticipation of the electrode being immersed in 0.1M dithiothreitol solution for an hour. The excess of dithiothreitol was washed off by using ultrapure water.⁷¹

This procedure was repeated for each solution to create each modified nanoparticle working electrode.

4.3: Electrochemical characterisation

Introduction

The electrochemical stability of the thiol SAM is determined by the equilibrium between the adsorbed thiol and the free thiolate. For example:⁸³



At negative potentials, thiols are reductively desorbed from the surface to a thiolate which is associated with, but not chemisorbed, to the electrode. Reductive desorption influences solution pH and electrode structure.

A typical potential for desorption of alkanethiols found in the literature is around 1.0 V (versus saturated calomel electrode, SCE), but this value may vary depending on the chemical structure of the thiol and on pH.^{84,85}

For each cyclic voltammetry, integration of the current involved in the electrodesorption peak gives the charge density (q) corresponding to the amount of chemisorbed species.⁸⁵

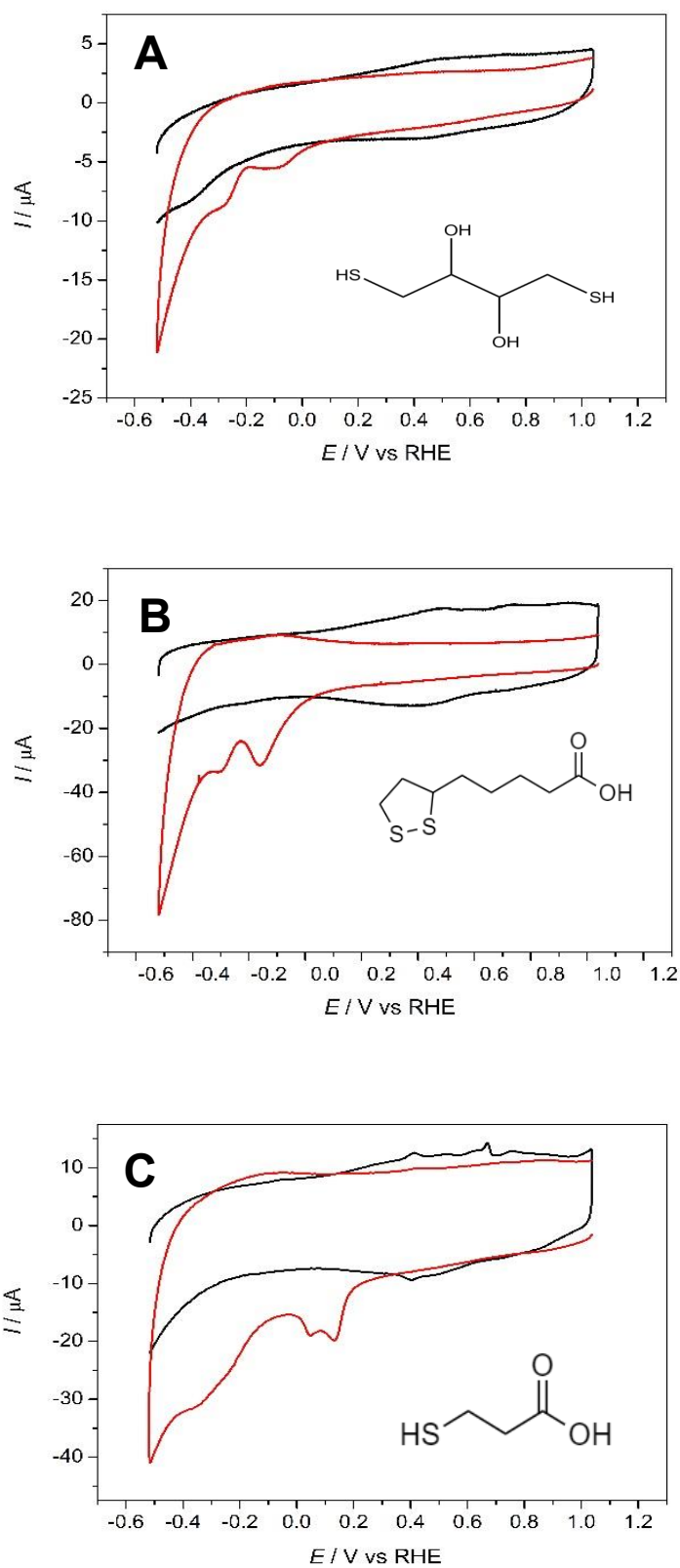


Figure 20 Voltammetric profile of gold nanoparticle supported glassy carbon electrode modified by (A) 1,4-dithiothreitol, (B) thioctic acid and (C) 3-mercaptopropionic acid. The black line shows gold nanoparticle scan after Pb UPD cleaning process.

The red scan shows the voltammetry of gold nanoparticle electrodes with adsorbed sulphides. Voltammetries were conducted in DPBS. Scan rate $\nu = 50 \text{ mV s}^{-1}$.

4.3.1: Electrochemical characterisation of 1,4-dithiothreitol

The physical characterisation of the functionalised gold nanoparticles was analysed electrochemically with cyclic voltammetry.

Figure 20A shows the voltammetric profile of the surface modified gold nanoparticle covered particles with 1,4-dithiothreitol. The blank voltammetry of the clean gold nanoparticles is included for comparison.

The surface modification was confirmed by cycling the working electrode to negative potentials to witness thiol desorption peaks at low potentials. The reduction peaks at lower potentials, -0.3 and -0.1 V vs RHE are associated to the irreversible desorption of DTT. When the electrode is then cycled in the positive direction, an additional broader peak is observed. This peak is related to thiol re-adsorption where the disulphide species are in close proximity after desorption and are then attracted to the surface and re-adsorb.

The reductive electrodesorption curves in the voltammetric profiles are a clear evidence of the presence of 1,4-dithiothreitol covalently attached to the gold nanoparticles.^{86,87}

DTT, 1,4-dithiothreitol is a short alkanedithiol with two hydroxyl groups that may provide an OH-rich surface, facilitating the lipid bilayers formation.⁸⁶ Previously observed DTT can self-organize on the Au (111) surface in a “lying-down” configuration, irrespective of the concentration and temperature.⁸⁵

It is possible to observe in a very negative potential a cathodic increase of the current density related to hydrogen evolution reaction (HER). The curve at negative potentials in the Figure 20A shows the cathodic polarization behaviour of DTT self-organized monolayer on Au (111), which corresponds to the reductive desorption of DTT.

4.3.1.1: Conclusion

The di-sulphide nature of DTT allows the double coordination of the molecule onto the surface of the gold nanoparticle electrode at lower potentials. Negative potentials are needed for the desorption of the molecule from the gold nanoparticle surface. This suggests that the S-Au bonds are strongly bound. Whilst this is not the most desirable molecule, it is also not the least desirable for the fundamental part of the sensor as it demonstrates characteristics of being stable when bound to the gold nanoparticles.

4.3.2: Electrochemical characterisation of Thioctic acid

Figure 20B shows the voltammetric profile of the surface modified gold nanoparticle covered particles with thioctic acid. The blank voltammetry of the clean gold nanoparticles is included for comparison. The changes in the voltammetric profiles are a clear indication of the presence of thioctic acid on the surface.

As the working electrode was cycled towards negative potentials, reduction peaks were seen at low potentials, -0.4 and -0.25 V vs RHE. When the electrode is cycled back to the positive direction, a defined peak is observed at -0.4 to -0.2 V vs RHE. This peak shows thiol re-adsorption where the disulphide molecules are in close enough range for attraction to still occur to the surface of the electrode, thus being able to re-adsorb onto the surface.

In this chapter, the gold nanoparticle covered working electrode was modified with thioctic acid. Cyclic voltammetry was used to confirm the surface had been successfully modified by the disulphide. By cycling the working electrode to negative potentials thiol, desorption occurred at low potentials, which were -0.4 and -0.25 V vs RHE, as well as re-adsorption in the same region on the positive scan. The desorption and re-adsorption peaks confirm that the working electrode had been modified by thioctic acid.

The thioctic acid as disulphide has two sulphur atoms which gives two attachment points to the gold nanoparticle electrode, which should offer higher stability. Therefore, desorption occurs at lower potentials.⁸⁸

4.3.1.1: Conclusion

It can be quantified that thioctic acid's two coordinating sulphur atoms, and presumed Van der Waals lateral interactions between hydrophobic aliphatic chains, give an improved stability when bound to the surface of the gold nanoparticles. Similarly to dithiothreitol, negative potentials are required for the reductive desorption. Thioctic acid, in comparison to the others, is the most stable sulphur containing molecule, and therefore is most desirable as the fundamental part of the sensor.

4.3.3: Electrochemical characterisation of 3- mercaptopropionic acid

Figure 20C shows the voltammetric profile of the surface modified gold nanoparticle covered particles with 3-mercaptopropionic acid (MPA). The blank voltammetry of the clean gold

nanoparticles is included for comparison. The changes in the voltammetric profiles are a clear evidence of the presence of 3-mercaptopropionic acid on the surface.

In Figure 20C, irreversible desorption peaks of 3- mercaptopropionic acid occur at lower potentials. Due to cycling the working electrode to negative potentials, these peaks are seen at -0.3, 0.2 and 0.1 V vs RHE. After cycling the working electrode to negative potentials, it is then cycled back in the positive direction, where re-adsorption peaks are observed. A small broad peak is observed, which corresponds to the re-adsorption of 3- mercaptopropionic acid onto the surface. The MPA desorbs at more positive scans, as seen in the literature, due to the less densely packed self-assembled monolayer (SAM).⁸⁸

4.3.1.1: Conclusion

Desorption of 3- mercaptopropionic acid at higher potential indicates that the Au-S bond is not as strongly bound to the surface as dithiothreitol and thioctic acid. This is due to 3- mercaptopropionic acid only having one Au-S bond, whereas the previous molecules have two sulphur atoms. 3- mercaptopropionic acid in comparison to the others di-sulphides, is the least stable sulphur containing molecule, and therefore is the least desirable as the fundamental part of the sensor.

Chapter 5: Conclusion and outlook:

The aim of this thesis was to demonstrate the electrochemical structure and stability of the three molecules: dithiothreitol, thiocetic acid and 3- mercaptopropionic acid. These sulphur containing molecules were analysed on a gold nanoparticle supported carbon electrode in physiological media. In each molecule, dithiothreitol, thiocetic acid and 3- mercaptopropionic acid, the decrease of the double layer charging current can be observed, as well as peaks associated to adsorption and desorption of the thiols.

The differences in desorption potentials between these molecules are evident, as the S-single and S-double containing molecules have different potential peak ranges, as well as the strength of the lateral interaction of the thiols, which result to different packing and coverage. . Throughout this report, it has been exhibited that S-single molecule 3- mercaptopropionic acid has desorption peaks at higher potentials. Whereas S-double containing molecules such as, dithiothreitol and thiocetic acid, desorb from the surface at lower potentials. The double coordination to the surface of the gold nanoparticles of dithiothreitol and thiocetic acid show an improved stability, as more negative potentials are needed for the desorption. In comparison, for the self-assembled mono layers of 3- mercaptopropionic acid, desorption at positive potentials is indicated, therefore not being as strongly bound to the surface as dithiothreitol and thiocetic acid.

The understanding of the stability of adsorbed sulphur containing molecules on gold electrodes in physiological conditions has immense potential for sensing. Therefore, they could lead to the controlled delivery of drugs in blood. The results obtained from this thesis give a clear indication that will contribute to the development and understanding of more robust and affordable electrochemical systems, such as electrochemical sensors.

References

- 1 R. Shanker, G. Singh, A. Jyoti, P. D. Dwivedi and S. P. Singh, in *Animal Biotechnology: Models in Discovery and Translation*, Elsevier, 2013, pp. 525–540.
- 2 J. Raba, M. a Fernández-baldo, S. V Pereira, G. a Messina and A. Franco, *Analytical biosensors for the pathogenic microorganisms determination*, 2013.
- 3 P. Leonard, S. Hearty, J. Brennan, L. Dunne, J. Quinn, T. Chakraborty and R. Kennedy, *Microb Technol* 32 CrossRef CAS, 2003, **32**, 3–13.
- 4 O. Lazcka, F. J. Del Campo and F. X. Muñoz, *Biosens. Bioelectron.*, 2007, **22**, 1205–1217.
- 5 R. Mistry, *Affordable ligand-based electrochemical detection of bacterial toxins*, 2017.
- 6 A. Chaubey and B. D. Malhotra, *Biosens. Bioelectron.*, 2002, **17**, 441–456.
- 7 C. Kaittanis, S. Santra and J. M. Perez, *Adv. Drug Deliv. Rev.*, 2010, **62**, 408–423.
- 8 T. M. Straub and D. P. Chandler, *J. Microbiol. Methods*, 2003, **53**, 185–197.
- 9 J. Monzó, I. Insua, F. Fernandez-Trillo and P. Rodriguez, *Analyst*, 2015, 7116–7128.
- 10 M. Nayak, A. Kotian, S. Marathe and D. Chakravorty, *Biosens. Bioelectron.*, 2009, **25**, 661–667.
- 11 C. Fournier-Wirth and J. Coste, *Biologicals*, 2010, **38**, 9–13.
- 12 F. Adzitey, N. Huda and G. R. R. Ali, *3 Biotech*, 2013, **3**, 97–107.
- 13 V. Velusamy, K. Arshak, O. Korostynska, K. Oliwa and C. Adley, *Biotechnol. Adv.*, 2010, **28**, 232–254.
- 14 D. Ivnitski, I. Abdel-Hamid, P. Atanasov and E. Wilkins, *Biosens. Bioelectron.*, 1999, **14**, 599–624.
- 15 E. Bakker and Y. Qin, *Anal. Chem*, 2006, **78**, 3965–3984.
- 16 A. Gencoglu and A. R. Minerick, *Microfluid. Nanofluidics*, 2014, **17**, 781–807.
- 17 D. Grieshaber, R. MacKenzie, J. Vörös and E. Reimhult, *Sensors*, 2008, **8**, 1400–1458.
- 18 P. D’Orazio, *Clin. Chim. Acta*, 2003, **334**, 41–69.
- 19 A. M. Villalba-rodr, R. Parra-saldivar and H. M. N. Iqbal, *Electrochemical Biosensors : A Solution to Pollution Detection with Reference to Environmental Contaminants*, .
- 20 H. Sierra, M. Cordova, C. S. J. Chen and M. Rajadhyaksha, *J. Invest. Dermatol.*, 2015, **135**, 612–615.
- 21 D. T. Buerk, *Biosensors: Theory and Applications.*, Publishing, Lancaster, 1993.
- 22 B. R. Egdins, *Chemical Sensors and Biosensors*, 2002.
- 23 W. Wróblewski, A. Dybko, E. Malinowska and Z. Brzózka, *Talanta*, 2004, **63**, 33–39.
- 24 S. Sukeerthi and A. Q. Contractor, 1994, **33**, 565–571.
- 25 K. Yagiuda, A. Hemmi, S. Ito, Y. Asano, Y. Fushinuki, C. Y. Chen and I. Karube, *Biosens. Bioelectron.*, 1996, **11**, 703–707.

- 26 I. Khan, K. Saeed and I. Khan, *Arab. J. Chem.*, 2019, **12**, 908–931.
- 27 A. Kumar and C. K. Dixit, *Methods for characterization of nanoparticles*, 2017.
- 28 D. Guo, G. Xie and J. Luo, *J. Phys. D. Appl. Phys.*, 2014, **47**.
- 29 P. Tiwari, K. Vig, V. Dennis and S. Singh, *Nanomaterials*, 2011, **1**, 31–63.
- 30 H. D. & P. N. P. Ken-Tye Yong, Mark T. Swihart, *Plasmonics*, 2009, **4**, 79–93.
- 31 M. Das, K. H. Shim, S. S. A. An and D. K. Yi, *Toxicol. Environ. Health Sci.*, 2011, **3**, 193–205.
- 32 S. Balakrishnan, F. A. Bhat and A. Jagadeesan, *Applications of gold nanoparticles in cancer*, 2017.
- 33 W. T. Liu, *J. Biosci. Bioeng.*, 2006, **102**, 1–7.
- 34 J. Riu, A. Maroto and F. X. Rius, *Talanta*, 2006, **69**, 288–301.
- 35 M. Brust, D. Bethell, C. J. Kiely and D. J. Schiffrin, *Langmuir*, 1998, **14**, 5425–5429.
- 36 Y. Yi-Cheun, B. Creran and V. Rotello, *NIH Public Acces*, 2014, **4**, 1871–1880.
- 37 M. Shah, V. Badwaik, Y. Kherde, H. K. Waghvani, T. Modi, Z. P. Aguilar, H. Rodgers, W. Hamilton, T. Marutharaj, C. Webb, M. B. Lawrenz and R. Dakshinamurthy, *Front. Biosci. (Landmark Ed.)*, 2014, **19**, 1320–44.
- 38 J. Valdez and I. Gómez, *J. Nanomater.*, 2016, **2016**, 7.
- 39 S. Omar, R., Naciri, A. E., Jradi, S., Battie, Y., Toufaily, J., Mortada, H., & Akil, *J. Mater. Chem.*, 2017, **5**, 10813 – 10821.
- 40 J. Cao, T. Sun and K. T. V. Grattan, *Sensors Actuators, B Chem.*, 2014, **195**, 332–351.
- 41 R. E. Ionescu, E. N. Aybeke, E. Bourillot, Y. Lacroute, E. Lesniewska, P. M. Adam and J. L. Bijeon, *Sensors (Switzerland)*, 2017, **17**.
- 42 R. Herizchi, E. Abbasi, M. Milani and A. Akbarzadeh, *Artif. Cells, Nanomedicine, Biotechnol.*, 2016, **44**, 596–602.
- 43 S. Sun, P. Mendes, K. Critchley, S. Diegoli, M. Hanwell, S. D. Evans, G. J. Leggett, J. A. Preece and T. H. Richardson, *Nano Lett.*, 2006, **6**, 345–350.
- 44 L. Srisombat, A. C. Jamison and T. R. Lee, *Colloids Surfaces A Physicochem. Eng. Asp.*, 2011, **390**, 1–19.
- 45 H. Bridle, *Nanotechnology for Detection of Waterborne Pathogens*, Elsevier, 2013.
- 46 S. Hebié, Y. Holade, K. Servat, B. K. Kokoh and T. W. Napporn, *Catal. Appl. Nano-Gold Catal.*, 2016.
- 47 M. Brust, M. Walker, D. Bethell, D. J. Schiffrin and R. Whyman, *J. Chem. Soc. Chem. Commun.*, 1994, 801–802.
- 48 K. Aslan and V. H. Pérez-Luna, *Langmuir*, 2002, **18**, 6059–6065.
- 49 N. G. Bastús, J. Comenge and V. Puntes, *Langmuir*, 2011, **27**, 11098–11105.
- 50 H. Erikson, A. Sarapuu, K. Tammeveski, J. Solla-Gullón and J. M. Feliu, *ChemElectroChem*, 2014, **1**, 1338–1347.

- 51 N. J. Ronkainen, H. B. Halsall and W. R. Heineman, *Chem. Soc. Rev.*, 2010, **39**, 1747.
- 52 J. Monzó, Y. Malewski, F. J. Vidal-Iglesias, J. Solla-Gullon and P. Rodriguez, *ChemElectroChem*, 2015, **2**, 958–962.
- 53 T. K. Sau and C. J. Murphy, *J. Am. Chem. Soc.*, 2004, **126**, 8648–8649.
- 54 J. Rodríguez-Fernández, J. Pérez-Juste, P. Mulvaney and L. M. Liz-Marzán, *J. Phys. Chem. B*, 2005, **109**, 14257–14261.
- 55 M. M. Behzadi S1, Ghasemi F, Ghalkhani M, Ashkarran AA, Akbari SM, Pakpour S, Hormozi-Nezhad MR, Jamshidi Z, Mirsadeghi S, Dinarvand R, Atyabi F, *Nanoscale.*, **7**, 5134–9.
- 56 E. Tomaszewska, K. Soliwoda, K. Kadziola, B. Tkacz-szczesna, G. Celichowski, M. Cichomski, W. Szmaja and J. Grobelny, *J. Nanomater.*, 2013, **2013**.
- 57 A. Kumar and C. K. Dixit, *Adv. Nanomedicine Deliv. Ther. Nucleic Acids*, 2017, 44–58.
- 58 I. W. Sudiarta and P. Chýlek, *Appl. Opt.*, 2002, **41**, 3545.
- 59 Y. Tang, X. Yu, J. Xu, B. Audit and S. Zhang, *Applications of Hybrid Nanoparticles in Biosensors*, Elsevier Inc., 2019.
- 60 V. Amendola and M. Meneghetti, *J. Phys. Chem. C*, 2009, **113**, 4277–4285.
- 61 D. Kumar, B. J. Meenan, I. Mutreja, R. D'Sa and D. Dixon, *Int. J. Nanosci.*, 2012, **11**.
- 62 S. Rahman, *Undergrad. J. Math. Model. One + Two*, 2016, **7**.
- 63 P. K. Ngumbi, S. W. Mugo and J. M. Ngaruiya, *IOSR J. Appl. Chem. (IOSR-JAC)*, 2018, **11**, 25–29.
- 64 M. Eguchi, D. Mitsui, H. L. Wu, R. Sato and T. Teranishi, *Langmuir*, 2012, **28**, 9021–9026.
- 65 D. A. C. Brownson and C. E. Banks, *The Handbook of Graphene Electrochemistry*, 2014.
- 66 J. Z. Aiping Yu, Victor Chabot, *Electrochemical Supercapacitors for Energy Storage and Delivery*, .
- 67 J. W. David Halliday, Robert Resnick, *Fundamentals of Physics*, .
- 68 N. Elgrishi, K. J. Rountree, B. D. McCarthy, E. S. Rountree, T. T. Eisenhart and J. L. Dempsey, *J. Chem. Educ.*, 2018, **95**, 197–206.
- 69 P. T. Kissinger and W. R. Heineman, *J. Chem. Educ.*, 1983, **60**, 702.
- 70 G. A. Mabbott, *J. Chem. Educ.*, 1983, **60**, 697.
- 71 A. Kolodziej, F. Fernandez-Trillo and P. Rodriguez, *J. Electroanal. Chem.*, 2017, 0–1.
- 72 C. Z. Allen J. Bard, *Electroanalytical Chemistry: A Series of Advances: Volume 24*, 2017.
- 73 D. E. Weisshaar and T. Kuwana, *Anal. Chem.*, 1985, **57**, 378–379.
- 74 J. Hernández, J. Solla-Gullón and E. Herrero, *J. Electroanal. Chem.*, 2004, **574**, 185–196.

- 75 Y. Chen, A. W. Hassel and A. Erbe, *Electrocatalysis*, 2011, **2**, 106–113.
- 76 J. Solla-Gullón and J. M. Feliu, *Curr. Opin. Electrochem.*, 2020, **22**, 65–71.
- 77 I. Electroanal and U. Milano, 1993, **321**, 353–376.
- 78 a P. C. and R. C. S. C. Vericat, a M. E. Vela, a G. Benitez, *Chem. Soc. Rev.*, 2010, 1805–1834.
- 79 S. Zhang, G. Leem, L. O. Srisombat and T. R. Lee, *J. Am. Chem. Soc.*, 2008, **130**, 113–120.
- 80 J. C. Love, L. A. Estroff, J. K. Kriebel, R. G. Nuzzo and G. M. Whitesides, *Self-Assembled Monolayers of Thiolates on Metals as a Form of Nanotechnology*, 2005.
- 81 W. W. Cleland, *Biochemistry*, 1964, **3**, 480–482.
- 82 J. J. Gooding, P. Erokhin and D. B. Hibbert, *Biosens. Bioelectron.*, 2000, **15**, 229–239.
- 83 N. S. Pesika, K. J. Stebe and P. C. Searson, *Langmuir*, 2006, **22**, 3474–3476.
- 84 T. Kawaguchi, H. Yasuda, K. Shimazu and M. D. Porter, *Langmuir*, 2000, **16**, 9830–9840.
- 85 M. B. Fritzen-Garcia, V. C. Zoldan, I. R. W. Z. Oliveira, V. Soldi, A. A. Pasa and T. B. Creczynski-Pasa, *Biotechnol. Bioeng.*, 2013, **110**, 374–382.
- 86 T. B. Creczynski-Pasa, M. A. D. Millone, M. L. Munford, V. R. de Lima, T. O. Vieira, G. a Benitez, A. a Pasa, R. C. Salvarezza and M. E. Vela, *Phys. Chem. Chem. Phys.*, 2009, **11**, 1077–1084.
- 87 D. Burshtain and D. Mandler, *Phys. Chem. Chem. Phys.*, 2006, **8**, 158–164.
- 88 E. Chow, D. B. Hibbert and J. J. Gooding, *Anal. Chim. Acta*, 2005, **543**, 167–176.
- 89 Gold Nanoparticles: Properties and Applications, <https://www.sigmaaldrich.com/technical-documents/articles/materials-science/nanomaterials/gold-nanoparticles.html>, (accessed 23 March 2018)

Appendix:

Sigma-Aldrich Reported Values: ⁸⁹

Diameter (nm)	SPR Peak Wavelength (nm)	Extinction Coefficient ($M^{-1}cm^{-1}$)
5	515-520	1.10×10^7
10	515-520	1.01×10^8
15	520	3.67×10^8
20	524	9.21×10^8
30	526	3.36×10^9
40	530	8.42×10^9
50	535	1.72×10^{10}
60	540	3.07×10^{10}
80	553	7.70×10^{10}
100	572	1.57×10^{11}